ACS Photonics

Article

pubs.acs.org/journal/apchd5

Plasmonic Enhancement of Single Photon Emission from a Site-Controlled Quantum Dot

Brandon Demory,[†] Tyler A. Hill,[‡] Chu-Hsiang Teng,[†] Lei Zhang,[‡] Hui Deng,[*,‡] and Pei-Cheng Ku[*,†]

[†]Department of Electrical Engineering and Computer Science and [‡]Department of Physics, The University of Michigan, Ann Arbor, Michigan 48109, United States

ABSTRACT: We showed enhanced single photon emission via exciton−plasmon coupling in a metal-encapsulated site-controlled quantum dot (QD) structure. It was observed that the average QD luminescence was enhanced by a factor of 7.33 ± 1.32 and the exciton lifetime was reduced by a factor of 12.8 ± 1.10. The exciton−plasmon coupling was enhanced by matching the exciton energy to the localized surface plasmon resonance. Due to the sensitivity of the plasmonic enhancement to dot-to-dot variations, measurements were performed on the same dot at different stages of the sample processing, enabled by the use of a novel site-controlled InGaN QD structure. This was then repeated over a large number of dots and compared between different metal materials to investigate the nature of the coupling.

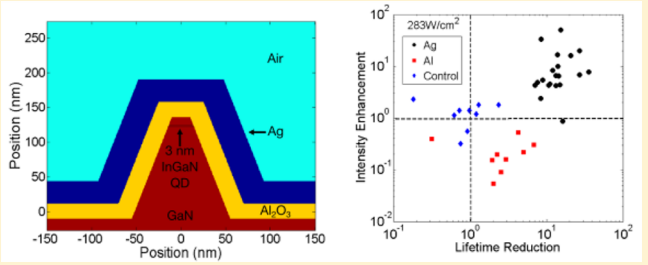

KEYWORDS: *plasmonic coupling, metallic cavity, quantum dots, III-nitride, single photon emission, site control*

On-demand, single-photon emission (SPE) has broad applications in quantum science and technologies. Epitaxial semiconductor quantum dots (QDs) intrinsically offer a higher repetition rate[1,2] than atoms,[3] molecules,[4] colloidal QDs,[5,6] and nitrogen vacancies (NV) in diamonds[7,8] and, therefore, are a good candidate for high-speed operations. Group III-nitride (III−N) QDs are of high interest due to their potential for SPE beyond cryogenic temperatures,[9,10] which is beneficial for practical deployment of quantum cryptography and low-power communications.[11] However, the strong piezoelectric field in strained III−N heterostructures can cause long radiative lifetimes on the order of tens of nanoseconds, limiting their operating speed to only tens of MHz.[12] The field also reduces the radiative efficiency due to the separation of electron and hole wave functions. Shortening the radiative lifetime can make III−N QDs faster and brighter. Photonic crystals[13−15] and metallic cavities[16−18] have been widely explored in III−V QD systems. Quantum dots coupled to these microcavities have shorter radiative lifetimes due to the Purcell effect, which is a result of the change in the local density of photonic states near the emitter.[19] The amount of change is proportional to Q/V, where Q is the cavity quality factor and V is the cavity mode volume. Light confinement in photonic crystal cavities can result in very high Q factors,[20] but require stringent control on QD cavity alignment.[14,15,21] The high Q factor inevitably produces a very narrow spectral enhancement window and hence small fabrication tolerance, which is even more challenging for short-wavelength III−N QDs.[14] In contrast, metallic cavities support plasmonic modes which have a very small mode volume. As a result, even with a small Q factor, a metallic cavity can still exhibit a strong Purcell effect. A small Q factor translates to a broadband enhancement, which reduces the fabrication complexity.[8] In this work, a silver (Ag)-based metallic cavity was coupled to InGaN QD-in-a-wire structures for enhanced SPE. The proposed structure, which took advantage of site-controlled InGaN QDs,[22] has the capability to be a highly integrable SPE source platform. The ordered QD array also enabled us to directly compare SPE from the same QD with and without the Ag cavity. This eliminates influences from any dot-to-dot variation occurring during QD growth and sample processing.

The cavity design is a dielectric spacer layer with an Ag layer on top. In the wavelength range of interest, there exists geometry-dependent localized surface plasmon resonances (LSPR) in Ag due to the shape formed from the metal layers on the QD pillar. An X−Z cross section of the cavity studied by the FDTD simulation is shown in Figure 1a.[23] More details about the simulation set up can be found in Demory.[24] All simulations were performed using room temperature dielectric constants. Data taken by Johnson and Christy[25] was used for the Ag parameters. The LSPR is well-studied[26−29] and is known to change with geometry.[28]

For core−shell structures there is hybridization[30] of the LSPR mode, causing a splitting of the single resonance into two at different resonance wavelengths, as shown in Figure 1b.[31,32] The high-energy resonance is an oscillation across the core within the shell.[32] In our structure, this results in a surface plasmon at the Ag−Al_2O_3 layer interface. Solving for the surface plasmon wavelength from the dispersion relation of a surface plasmon polariton at the interface between a metal and a dielectric using the Ag parameters and the measured index of refraction (n = 1.66) of Al_2O_3 from the experiment yields a

Received: February 25, 2015
Published: July 27, 2015

DOI: 10.1021/acsphotonics.5b00086
ACS Photonics 2015, 2, 1065−1070

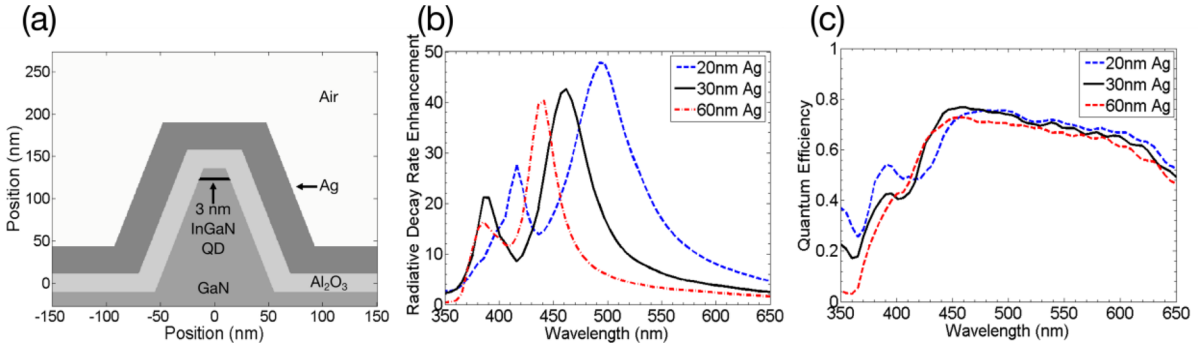

Figure 1. (a) X−Z cross section schematic of a 25 nm top diameter InGaN/GaN QD pillar inside a 30 nm Ag cavity. The cavity is radially symmetric. (b) Simulated radiative decay rate enhancement for silver thicknesses of 20, 30, and 60 nm. The resonance peak of the cavity blue shifts as the silver thickness is increased. (c) Cavity quantum efficiency of the decay rate enhancement for silver thicknesses of 20, 30, and 60 nm. The values are the fraction of the total decay rate enhancement that is due to radiative enhancement. The lower-energy resonance always has higher quantum efficiency.

surface plasmon wavelength of approximately 390 nm, which agrees with the high-energy peak in Figure 1b. The low-energy (long-wavelength) resonance is an oscillation across the outer surface shell. By increasing the thickness of the Ag film, the low-energy resonance can be blue-shifted toward the high-energy (short-wavelength) peak. In the limit of an infinitely thick silver film, the two resonances converge toward a single resonance of a metallic void, whose resonance wavelength is in between the two resonances of the shell structure.[32] The ability to tune this resonance peak is shown in Figure 1b from an Ag thickness of 20−60 nm. The calculated Q-factor, $Q = \omega_{max}/\Delta\omega_{fwhm}$ of this resonance peak for the three metal film thicknesses of 20, 30, and 60 nm is 6.8, 8.9, and 12.6, respectively. The resulting cavity antenna quantum efficiency (AQE) of the decay rate enhancement is shown in Figure 1c. The low-energy resonance has a higher quantum efficiency, which is expected of the lowest order resonance. The QDs used in this work had emission in the wavelength range of 410−420 nm, which is the wavelength regime where the two resonances overlap. This results in a coupled mode with quantum efficiency lower than the quantum efficiency of the low-energy mode.

The InGaN/GaN QDs were fabricated by a top-down approach from InGaN/GaN quantum wells (QWs). The schematic of the resulting QD pillar from the fabrication procedure described below is shown in Figure 2a. The QW wafer was grown by metal−organic chemical vapor deposition (MOCVD) on a (0001)-oriented sapphire substrate.

A single 3 nm thick InGaN QW with an emission wavelength of 470 nm was grown on top of a 1.5-μm GaN layer and capped with a 10 nm GaN layer. All layers were unintentionally n-typed doped at a concentration of approximately 3×10^{16} (cm^{-3}). Using electron-beam lithography and inductively coupled plasma reactive ion etching (ICP-RIE), the location and diameter of the QD pillars were defined. The height of the pillars was controlled at 135 nm. The air/InGaN interface generates the lateral confinement for excitons via a combination of strain relaxation and band bending due to surface depletion. A scanning electron microscope (SEM) image of an array of ordered 28 nm top diameter QD pillars coated in 20 nm of Al_2O_3 is shown in Figure 2b. More details of the QD fabrication, verification by second order correlation measurements, and optical properties can be found in Lee[22] and Zhang.[33−35] To form the Ag LSPR cavity, the QD array was first coated with 20 nm of Al_2O_3 by atomic layer deposition at 250 °C with a rate of 1.05 Å/s, followed by Ag deposition.

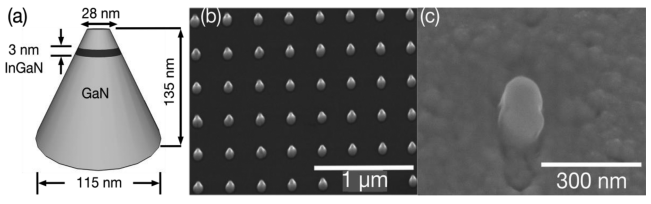

Figure 2. (a) Structural schematic of a 28 nm diameter InGaN QD inside GaN nanopillar. (b) SEM bird's eye view image of a 28 nm QD dense array coated in 20 nm Al_2O_3. (c) SEM bird's eye view image of a single QD coated with the 30 nm Ag cavity.

For measurements, we used a confocal microscopy setup for single QD spectroscopy. Each QD was optically excited from the front (metal) side of the sample with a 390 nm wavelength femtosecond pulse focused to a 30 μm spot, incident 55° from normal incidence. The photoluminescence (PL) signal was collected using a 0.6 NA objective on the same side as the incident light. All measurements were performed at 10 K. More details about the measurement setup can be found in Zhang.[34]

The sample was divided into three sections: Ag section, aluminum (Al) section, and a control section of just Al_2O_3. The Ag section was used to demonstrate the SPE enhancement by LSPR. To rule out the source of the enhancement due to non-LSPR effects such as metal reflection, the Al section was included. In the QD emission wavelength range, there is no expected LSPR for the Al cavity, but aluminum has similar reflectivity as Ag. Therefore, if the source of the enhancement is metal reflection, both sections would give comparable results. The control section of Al_2O_3 was included as an unchanged section, measured during each measurement stage to adjust for any possible intensity variation of different measurement days.

The Ag and Al cavities were deposited using electron-beam evaporators with the sample mounted at a 60° angle with respect to the molecular beam direction. Initially, 307 Å of film were deposited at a rate of 5 Å/s. The sample was then rotated 180° and another 307 Å of metal were deposited. While rotating the sample halfway through the deposition improved the conformity of the metal film by reducing shadowing effects, the conical sidewall coverage is still imperfect. An SEM of a single dot in the 30 nm Ag cavity deposited by the two-step angled deposition is shown in Figure 2c. Measurements were taken from individual QDs in each section before and repeated on the same QDs after the metal processing.

DOI: 10.1021/acsphotonics.5b00086
ACS Photonics 2015, 2, 1065−1070

The exciton emission spectra under pulsed excitation of a single QD with and without the Ag cavity are shown in Figure 3a,b for two excitation intensities: 283 and 707 W/cm^2. With

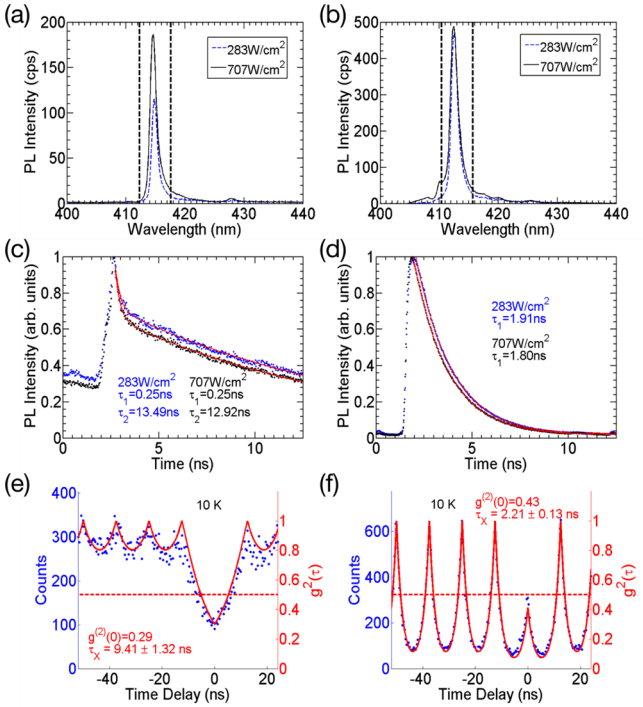

Figure 3. Optical measurements of a single QD taken at 10 K before and after the deposition of the silver cavity for two excitation intensities, 283 (blue) and 707 W/cm^2 (black). (a) PL intensity taken initially and (b) the enhanced PL intensity after the cavity deposition. Dotted lines indicate position of the spectral filter used for the time-resolved PL and autocorrelation measurements. (c) TRPL intensity taken initially and fit with a biexponential function. The functional weighting of τ_1 and τ_2 are 0.23 (0.71) for 283 W/cm^2 and 0.26 (0.66) for 707 W/cm^2. (d) TRPL intensity taken after the cavity deposition. τ = 1.91 and 1.80 ns at the respective intensities. The weighting of the second exponential term was negligible, thus, only one lifetime is given. (e) Autocorrelation $g^{(2)}$ measurement of the QD before the cavity, measured with an excitation intensity of 707 W/cm^2 without background subtraction. The fitting (red) gives a $g^{(2)}(0)$ value of 0.29 and a lifetime τ = 9.41 ± 1.32 ns. (f) Autocorrelation with the cavity, showing maintained single photon emission, and a $g^{(2)}(0)$ value of 0.43 with a reduced lifetime of τ = 2.21 ± 0.13 ns.

the Ag cavity, the integrated intensities of the exciton PL are 4.28 ± 0.001 and 3.25 ± 0.001 times brighter for each excitation intensity, respectively. The time-resolved photoluminescence (TRPL) intensities for the QD with and without the silver cavity at the two excitation intensities are shown in Figure 3c,d. The QDs exhibited two distinct lifetimes before Ag deposition: a shorter component on the order of ~250 ps, and a longer component on the order of nanoseconds associated with the exciton emission. The TRPL data was fitted with a biexponential decay function in order to quantify the magnitude of each lifetime component in the collected signal. In Figure 3c, at the respective excitation intensities of 283 W/cm^2 (707 W/cm^2), τ_1 = 0.25 ns (0.25 ns) with a weighting of 0.25 (0.26) and τ_2 = 13.5 ns (12.9 ns) with a weighting of 0.71 (0.66). After the cavity deposition, there was only one TRPL lifetime of τ = 1.91 ns (1.80 ns) seen in Figure 3d, as the weighting of the second term was negligible.

The SPE properties of the InGaN QD were confirmed by measurement of the second-order photon correlation function $g^{(2)}$ with a Hanbury-Brown and Twiss (HBT) interferometer. The $g^{(2)}$ function shows clear antibunching without background subtraction both with and without the Ag cavity, as shown in Figure 3e,f. The fitting yields $g^{(2)}(0)$ values of 0.29 and 0.43, respectively, demonstrating SPE was preserved with the cavity.[34] The increase in the $g^{(2)}$ value with Ag is due to the broadband enhancement of the background emission. The QD lifetime can also be determined from exponential fitting of the side peaks of the $g^{(2)}$ function. It is seen that the lifetime of the QD was reduced by 4.3 ± 0.6 times from 9.41 ± 1.32 ns to 2.21 ± 0.13 ns after metal deposition. The peaks became better separated in the measurement with the Ag cavity as the lifetime became much shorter than the 12.5 ns repetition rate of the laser.

The origin of the shorter lifetime component in the initial QD measurements was unclear; however, it was not the main contributor to the SPE, as evidenced by the $g^{(2)}$ measurement. Additionally, the intensity of the shorter lifetime component was less than 1/3 of the long lifetime component's intensity. Therefore, we calculated the lifetime reduction ratio based only on the long lifetime component. From Figure 3c,d, the lifetime reduction ratio for this QD was 7.1 ± 0.02 times at 283 W/cm^2 and 7.2 ± 0.02 times at 707 W/cm^2.

The ratio of the PL intensity enhancement S^{new}/S^0 and QD lifetime reduction ($\tau^0_{tot}/\tau^{new}_{tot}$) for each QD measured in the respective sections are shown in Figure 4 at excitation intensity

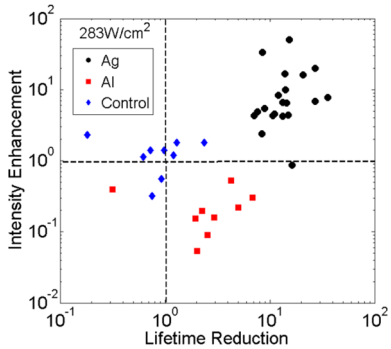

Figure 4. Total lifetime reduction and integrated intensity enhancement for each individual dot measured with an excitation intensity of 283 W/cm^2. The (black) circles represent the Ag cavity, the (red) squares represent the Al cavity, and the (blue) diamonds represent the control. Values less than 1 indicate a reduction in intensity or the lifetime increasing, respectively. The dotted lines represent no change in the parameter for the respective axes, and their intersection indicates the point of an unchanged dot.

of 283 W/cm^2. Here, "S" is the emission intensity and "τ" is the measured TRPL lifetime, with the superscripts "0" and "new" representing before and after applying metal coating to the Al_2O_3-coated QD.

In Figure 4, when the QDs were excited at 283 W/cm^2, we can see that the Ag cavity simultaneously increased the QD emission intensity and reduced the lifetime, signifying enhancement of the spontaneous emission rate. Although the QD emission is off of the cavity resonance, as suggested in Figure 1b, there is still enhancement due to the broad nature of the resonance peak. The average intensity enhancement for 20 QDs in the Ag section is 10.9 ± 2.6 times and the average

DOI: 10.1021/acsphotonics.5b00086
ACS Photonics 2015, 2, 1065−1070

lifetime reduction is 15.0 ± 1.6 times. The larger lifetime reduction factor compared to the intensity enhancement is attributed to additional nonradiative recombination in the Ag cavity.

These results were contrasted in the aluminum section, where both the integrated intensity and total lifetime were reduced by 0.23 ± 0.04 times and 3.13 ± 0.61 times, respectively. Both Ag and Al are highly reflective in this wavelength regime; thus, this result rules out enhancement due to a mirror effect. For the control section, some of the QDs showed slight changes in the lifetime, as shown in Figure 4 lifetime reduction ratio variations. Over time, the shorter lifetime component of the QD from the biexponential fitting becomes more weighted. The origins of the shorter lifetime component and its changes over time are unknown and under further investigation. In addition, the initial exciton lifetimes of interest are on the order of the repetition time of the laser (12.5 ns). Because of this, the fitting of the longer lifetime component is more susceptible to fluctuations between measurement days, which can result in lifetime variations.

In addition to the intensity enhancement and lifetime reduction, we examined the saturation properties of the QDs before and after the metal cavity deposition. Figure 5 shows the

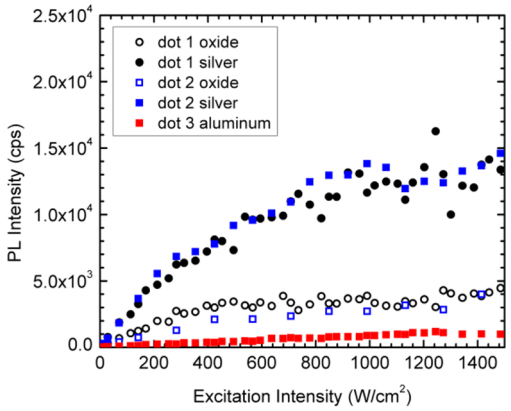

Figure 5. Saturation curves for a two individual QDs measured before (open marker) and after (filled marker) the silver cavity deposition. Two different Integrated Intensity saturation levels demonstrate the enhanced radiative process in the QD. The saturation curve for an aluminum coated QD is given as a reference.

PL intensity as a function of the excitation intensity for two QDs measured before and after Ag deposition and the PL intensity of a QD coated with the aluminum cavity for reference. The oxide coated QDs saturate above 707 W/cm^2, which we define as the saturation pumping intensity I_{sat}. The two different saturation levels for the QDs with and without the cavity signify the enhancement in the emission process. The lower saturation emission intensity level for the Al QD shows the non-LSPR effects that reduce the TRPL lifetime also reduce the PL intensity.

The difference in the enhancement between the two metals confirmed that the mechanism for the enhanced SPE is the Purcell effect due to the effective Ag plasmonic cavity. The enhancement is due to coupling between the QDs and the plasmonic resonance of the Ag. The change in the radiative decay rate Γ_{rad} can be quantified using the radiative Purcell factor F_p as

$$\Gamma_{rad}^{new} = F_p \times \Gamma_{rad}^{0} \tag{1}$$

The Purcell factor is the ratio of the initial radiative lifetime before the cavity to the new radiative lifetime after the cavity resonator. In addition to the modification in the radiative decay rate, there will be a change in the emission intensity from the QD,[27] which can be written as

$$\frac{S^{new}}{S^0} = \frac{\xi^{new}}{\xi^0} \times \frac{f^{new}(I)}{f^0(I)} \times \frac{R^{new}}{R^0} \times \frac{\eta^{new}}{\eta^0} \tag{2}$$

"S" is the emission intensity, "ξ" is the collection efficiency, "$f(I)$" is the QD exciton occupation probability, "R" is the QD decay rate, and "η" is the emitter quantum efficiency (QE). The collection efficiency ratio (ξ^{new}/ξ^0) measures how the angular distribution of the emission changes due to the addition of the cavity with respect to the collection optics. The collection efficiency depends on the measurement position, emission angle, and collection angle (numerical aperture or NA). The collection efficiency ratio is the ratio of the collection efficiency of the two measurement steps. The factor $f(I)$ is the probability the QD is excited into its excitonic state when the QD is empty and the laser pulse hits. $f(I)$ increases with the excitation intensity I_{exc} inside the QD and will reach unity at the saturation intensity I_{sat} once the excitonic state has been filled and not given enough time to decay. The QE ratio can be related to the Purcell factor and QD lifetime via

$$\frac{\eta^{new}}{\eta^0} = F_p \times \frac{\tau_{tot}^{new}}{\tau_{tot}^{0}} \tag{3}$$

($R \times \eta$) is the rate the QD generates photons. Under continuous-wave excitation, R is simply the inverse of the QD lifetime τ_{tot}. But under pulsed excitation, R is limited by the laser repetition rate R_{laser}. Since the excitonic state of the QD can only be refilled if it is empty when a laser pulse hits, the intensity measured from PL depends on both R_{laser} and τ_{tot}. For a QD with a lifetime τ_{tot} much shorter than the laser repetition time ($1/R_{laser}$), the QD is empty when each new laser pulse arrives, thus, R is simply R_{laser}, which is (1/12.5 ns) in this case. However, for QDs with lifetimes on the order of or greater than ($1/R_{laser}$), R can be written as

$$\frac{1}{R} = \sum_{n=1}^{\infty} \left(p_n \times \frac{n}{R_{laser}} \right) \tag{4}$$

where "n" is the n-th repetition interval during which the QD decays and p_n is the associated probability. p_n can be determined using the time-resolved PL data. We obtained the R^{new}/R^0 ratio at 283 W/cm^2 to range between 1.4−3.2 and at 707 W/cm^2 to range between 1.4−2.8.

To study the change in the PL intensity enhancement ratio with the Ag cavity above I_{sat}, we measured the QDs emission enhancement and lifetime reduction ratios at 707 W/cm^2, shown in Figure 6. When the excitation intensity was increased to 707 W/cm^2, the average PL intensity enhancement ratio is 7.33 ± 1.32, which is 30% lower than 10.9 ± 2.6 obtained at 283 W/cm^2 (Figure 4). This is because at 707 W/cm^2, both $f^{Ag}(I)$ and $f^0(I)$ saturated at unity as evidenced by the saturated PL intensity obtained from excitation intensity dependent measurements in Figure 5. At 283 W/cm^2, $f^{Ag}(I)/f^0(I)$ can be obtained by taking the ratio of eq 2 for the two excitation powers, using the experimental PL and TRPL enhancement ratios, eq 4 to determine R^{Ag}/R^0 at each intensity, and the fact that the collection efficiency ratio is intensity independent. We obtained $f^{Ag}(I)/f^0(I)$ at 283 W/cm^2 to range between 0.4−1.8

DOI: 10.1021/acsphotonics.5b00086
ACS Photonics 2015, 2, 1065−1070

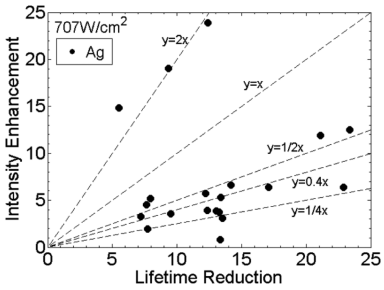

Figure 6. Total lifetime reduction and integrated intensity enhancement for each Ag cavity QD measured with an excitation intensity of 707 W/cm^2. Values less than 1 indicate a reduction in intensity or the lifetime increasing, respectively. Dotted guidelines show the intensity enhancement "*y*" as a function of the lifetime reduction "*x*".

for the 20 QDs with only 5 QD with values below 1. Therefore, the intensity enhancement ratio reduction is directly related to the reduction of $f^{Ag}(I)/f^{0}(I)$ to unity above the saturation intensity.

The enhancement values shown in Figure 6 are due solely to the improved radiative process. Using the linear guidelines in Figure 6, the QDs seem to fall into two distinct regimes: the first region where the intensity enhancement is a fraction of the lifetime reduction, and the second region where the intensity enhancement scales as twice the lifetime reduction. At saturation, the intensity change should be proportional to eq 2, with $f^{Ag}(I)/f^{0}(I)$ equal to unity.

The first regime results are what we expect for a cavity with a cavity AQE less than 1, such as this metallic cavity. Part of the lifetime reduction is due to metal Joule losses, which are responsible for the low AQE of the cavity. At the average emission wavelength of 411 nm, the simulated cavity antenna quantum efficiency AQE for 30 nm Ag is 0.47, from Figure 1c. For QDs with close to unity QE, the QE after the metallic cavity will approach the upper bound AQE. Most of these QDs were relatively bright initially, signaling higher initial QE due to the proportionality of the two quantities. Thus, considering only lifetime change and emission intensity change above the saturation intensity, we expect the data to show a fractional slope relationship in Figure 5, as the AQE is less than unity for a metallic cavity.

In the second regime, the intensity change implies that the dots either had very low QE initially or were not fully saturated at the excitation intensity of 707 W/cm^2. The former is more likely, as these three QDs correspond to QDs with dimmed initial PL intensity. Intensity enhancement here is due to an improved QE for the emitter with the cavity structure over without the cavity. Even though enhancement using a metallic structure introduces another nonradiative channel due to metal losses, a net increase in QE is possible for an emitter that does not start with an initial QE of 1.

Because the QDs have less than unity QE both before and after the cavity, F_p cannot be calculated directly by taking the ratio of the measured lifetimes. Since we cannot measure the radiative lifetimes directly and are using a pulsed excitation system, the Purcell factor, F_p for all of the QDs can be calculated by substitution of eq 3 into eq 2, using the experimental ratios from the excitation intensity 707 W/cm^2, and neglecting the collection efficiency ratio. From simulation, the collection efficiency ratio is less than unity as the cavity reduces the collectable emission. So, the experimental F_p is a floor for the true Purcell factor. The results are shown in Figure 7 together with the QD PL intensities before embedding them into the Ag cavities.

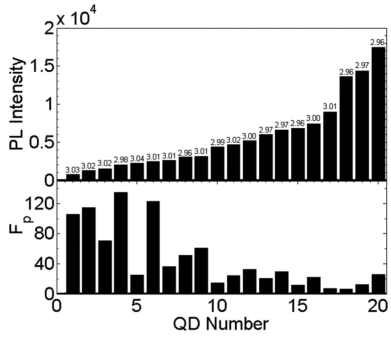

Figure 7. Initial measured PL intensity for the oxide coated QDs and the calculated Purcell factor in the cavity at the excitation intensity of 707 W/cm^2. The dots are in order of PL intensity emission collected initially from left to right. Labeled above is the corresponding PL peak energy in eV. The dimmest dots have the largest photon energy, indicating smaller QD size. Smaller QDs received the largest enhancement and have a larger F_p.

The Purcell factor at the excitation intensity of 707 W/cm^2 has an average value of 46 ± 9.0, with a fractional error of less than 5% for each individually calculated F_p. In Figure 7, the PL intensities are sorted from the QD with the lowest initial measured PL intensity to QD with the highest. The corresponding QD emission energy is listed above the bar for each QD. Most of the initially dimmed QDs have larger emission energies, which is a result of smaller QD diameters. Slightly smaller QDs have a larger surface-to-volume ratio, exhibiting lower QEs due to enhanced surface recombinations. The QDs that were initially dim received the largest change in brightness, corresponding to the larger F_p. However, according to our numerical calculations, small variations in the QD diameter and thickness on the order of 10% do not result in a large change in the enhancement, as observed in Figure 7. The origin of the correlation between the large variation of F_p and initial QD QEs requires further investigations.

In summary, we have demonstrated enhanced SPE in InGaN QDs is possible with a simple, Ag film cavity. These results are significant as they show the simultaneous enhancement of many QDs with a single cavity coating across a large area, which has a large practical significance over other methods that involve a cavity to be placed around individual dots. Although all measurements were taken at low temperature, high temperature operation is possible by increasing the band offset of the active region, for example, AlGaN barrier. This cavity design can be a foundation for on-chip enhanced single photon emitters in the ultraviolet/visible range. Due to the broad enhancement peak of the Ag cavity, this design is suitable for enhancing emission across a ∼100 nm width of the visible spectrum.

AUTHOR INFORMATION

Corresponding Authors

*E-mail: peicheng@umich.edu. Phone: +1(734)-764-7134.
*E-mail: dengh@umich.edu. Phone: +1(734)-763-7835.

Notes

The authors declare no competing financial interest.

DOI: 10.1021/acsphotonics.5b00086
ACS Photonics 2015, 2, 1065−1070

■ ACKNOWLEDGMENTS

We acknowledge the support by the National Science Foundation (NSF) under Awards ECCS 0901477 (for growth), ECCS 1102127 (for fabrication and measurements), and DMR 1120923 (for theory). Part of the fabrication work was performed in the Lurie Nanofabrication Facility (LNF), which is part of the NSF NNIN network.

■ REFERENCES

(1) Jarjour, A. F.; Oliver, R. A.; Taylor, R. A. Nitride-based quantum dots for single photon source applications. *Phys. Status Solidi A* **2009**, *206*, 2510−2523.
(2) Michler, P.; Kiraz, A.; Becher, C.; Schoenfeld, W. V.; Petroff, P. M.; Zhang, L. D.; Hu, E.; Imamoglu, A. A quantum dot single-photon turnstile device. *Science* **2000**, *290*, 2282−2285.
(3) Buluta, I.; Ashhab, S.; Nori, F. Natural and artificial atoms for quantum computation. *Rep. Prog. Phys.* **2011**, *74*, 1−16.
(4) Lounis, B.; Moerner, W. E. Single photons on demand from a single molecule at room temperature. *Nature* **2000**, *407*, 491−493.
(5) Brokmann, X.; Coolen, L.; Dahan, M.; Hermier, J. P. Measurement of the radiative and nonradiative decay rates of single CdSe nanocrystals through a controlled modification of their spontaneous emission. *Phys. Rev. Lett.* **2004**, *93*, 107403.
(6) De Vittorio, M.; Pisanello, F.; Martiradonna, L.; Qualtieri, A.; Stomeo, T.; Bramati, A.; Cingolani, R. Recent advances on single photon sources based on single colloidal nanocrystals. *Opto-Electron. Rev.* **2010**, *18*, 1−9.
(7) Jelezko, F.; Wrachtrup, J. Single defect centres in diamond: A review. *Phys. Status Solidi A* **2006**, *203*, 3207−3225.
(8) Choy, J. T.; Hausmann, B. J. M.; Babinec, T. M.; Bulu, I.; Khan, M.; Maletinsky, P.; Yacoby, A.; Loncar, M. Enhanced single-photon emission from a diamond-silver aperture. *Nat. Photonics* **2011**, *5*, 738−743.
(9) Holmes, M. J.; Choi, K.; Kako, S.; Arita, M.; Arakawa, Y. Room-Temperature Triggered Single Photon Emission from a III-Nitride Site-Controlled Nanowire Quantum Dot. *Nano Lett.* **2014**, *14*, 982−986.
(10) Kako, S.; Santori, C.; Hoshino, K.; Gotzinger, S.; Yamamoto, Y.; Arakawa, Y. A gallium-nitride single-photon source operating at 200K. *Nat. Mater.* **2006**, *5*, 887−892.
(11) Shields, A. J. Semiconductor quantum light sources. *Nat. Photonics* **2007**, *1*, 215−223.
(12) Brassard, G.; Bennett, C. H. Quantum Cryptography. *Lect. Notes Comput. Sci.* **1988**, *325*, 79−90.
(13) Rao, V.; Hughes, S. Single quantum dot spontaneous emission in a finite-size photonic crystal waveguide: Proposal for an efficient "on chip" single photon gun. *Phys. Rev. Lett.* **2007**, *99*, 193901.
(14) Hennessy, K.; Badolato, A.; Winger, M.; Gerace, D.; Atature, M.; Gulde, S.; Falt, S.; Hu, E. L.; Imamoglu, A. Quantum nature of a strongly coupled single quantum dot-cavity system. *Nature* **2007**, *445*, 896−899.
(15) Tandaechanurat, A.; Ishida, S.; Guimard, D.; Nomura, M.; Iwamoto, S.; Arakawa, Y. Lasing oscillation in a three-dimensional photonic crystal nanocavity with a complete bandgap. *Nat. Photonics* **2011**, *5*, 91−94.
(16) Akimov, A. V.; Mukherjee, A.; Yu, C. L.; Chang, D. E.; Zibrov, A. S.; Hemmer, P. R.; Park, H.; Lukin, M. D. Generation of single optical plasmons in metallic nanowires coupled to quantum dots. *Nature* **2007**, *450*, 402−406.
(17) Russell, K. J.; Liu, T. L.; Cui, S. Y.; Hu, E. L. Large spontaneous emission enhancement in plasmonic nanocavities. *Nat. Photonics* **2012**, *6*, 459−462.
(18) Hofmann, C. E.; de Abajo, F. J. G.; Atwater, H. A. Enhancing the Radiative Rate in III-V Semiconductor Plasmonic Core-Shell Nanowire Resonators. *Nano Lett.* **2011**, *11*, 372−376.
(19) Purcell, E. M. Spontaneous emission probabilities at radio frequencies. *Phys. Rev.* **1946**, *69*, 681−681.
(20) Vahala, K. J. Optical microcavities. *Nature* **2003**, *424*, 839−846.
(21) Ellis, D. J. P.; Bennett, A. J.; Dewhurst, S. J.; Nicoll, C. A.; Ritchie, D. A.; Shields, A. J. Cavity-enhanced radiative emission rate in a single-photon-emitting diode operating at 0.5 GHz. *New J. Phys.* **2008**, *10*, 043035.
(22) Lee, L. K.; Ku, P. C. Fabrication of site-controlled InGaN quantum dots using reactive-ion etching. *Phys. Status Solidi C* **2012**, *9*, 609−612.
(23) Lumerical Solutions, Inc.; http://www.lumerical.com/tcad-products/fdtd/.
(24) Demory, B.; Hill, T.; Teng, C. H.; Zhang, L.; Ku, P.-C. Enhancement of Spontaneous Emission Rate in an InGaN Quantum Dot Coupled to a Plasmonic Cavity. *CLEO*; Optical Society of America: San Jose, California, 2013; p QF1A.3.
(25) Johnson, P. B.; Christy, R. W. Optical constants of noble metals. *Phys. Rev. B* **1972**, *6*, 4370−4379.
(26) Liaw, J. W.; Chen, J. H.; Chen, C. S.; Kuo, M. K. Purcell effect of nanoshell dimer on single molecule's fluorescence. *Opt. Express* **2009**, *17*, 13532−13540.
(27) Bharadwaj, P.; Novotny, L. Spectral dependence of single molecule fluorescence enhancement. *Opt. Express* **2007**, *15*, 14266−14274.
(28) Mock, J. J.; Barbic, M.; Smith, D. R.; Schultz, D. A.; Schultz, S. Shape effects in plasmon resonance of individual colloidal silver nanoparticles. *J. Chem. Phys.* **2002**, *116*, 6755−6759.
(29) Chowdhury, M. H.; Pond, J.; Gray, S. K.; Lakowicz, J. R. Systematic computational study of the effect of silver nanoparticle dimers on the coupled emission from nearby fluorophores. *J. Phys. Chem. C* **2008**, *112*, 11236−11249.
(30) Sihvola, A. Character of surface plasmons in layered spherical structures. *Prog. Electromagn. Res.* **2006**, *62*, 317−331.
(31) Prodan, E.; Nordlander, P. Structural tunability of the plasmon resonances in metallic nanoshells. *Nano Lett.* **2003**, *3*, 543−547.
(32) Prodan, E.; Radloff, C.; Halas, N. J.; Nordlander, P. A hybridization model for the plasmon response of complex nanostructures. *Science* **2003**, *302*, 419−422.
(33) Zhang, L.; Lee, L. K.; Teng, C. H.; Hill, T. A.; Ku, P. C.; Deng, H. How much better are InGaN/GaN nanodisks than quantum wells-Oscillator strength enhancement and changes in optical properties. *Appl. Phys. Lett.* **2014**, *104*, 051116.
(34) Zhang, L.; Teng, C. H.; Hill, T. A.; Lee, L. K.; Ku, P. C.; Deng, H. Single photon emission from site-controlled InGaN/GaN quantum dots. *Appl. Phys. Lett.* **2013**, *103*, 192114.
(35) Zhang, L.; Hill, T. A.; Teng, C.-H.; Demory, B.; Ku, P.-C.; Deng, H. Carrier dynamics in site- and structure-controlled InGaN/GaN quantum dots. *Phys. Rev. B: Condens. Matter Mater. Phys.* **2014**, *90*, 245311.

DOI: 10.1021/acsphotonics.5b00086
ACS Photonics 2015, 2, 1065−1070